atmosphere

MDPI

Article

Sensitivity Analysis and Performance Evaluation of the WRF Model in Forecasting an Extreme Rainfall Event in Itajubá, Southeast Brazil

Denis William Garcia, Michelle Simões Reboita * and Vanessa Silveira Barreto Carvalho

Instituto de Recursos Naturais, Universidade Federal de Itajubá, UNIFEI, Av. BPS, 1303, Itajubá 37500-903, MG, Brazil; denisevolution98@unifei.edu.br (D.W.G.); vanessa.silveira@unifei.edu.br (V.S.B.C.)
* Correspondence: reboita@unifei.edu.br

Abstract: On 27 February 2023, the municipality of Itajubá in southeastern Brazil experienced a short-duration yet high-intensity rainfall event, causing significant socio-economic impacts. Hence, this study evaluates the performance of the Weather Research and Forecasting (WRF) model in simulating this extreme event through a set of sensitivity numerical experiments. The control simulation followed the operational configuration used daily by the Center for Weather and Climate Forecasting Studies of Minas Gerais (CEPreMG). Additional experiments tested the use of different microphysics schemes (WSM3, WSM6, WDM6), initial and boundary conditions (GFS, GDAS, ERA5), and surface datasets (sea surface temperature and soil moisture from ERA5 and GDAS). The model's performance was evaluated by comparing the simulated variables with those from various datasets. We primarily focused on the representation of the spatial precipitation pattern, statistical metrics (bias, Pearson correlation, and Kling–Gupta Efficiency), and atmospheric instability indices (CAPE, K, and TT). The results showed that none of the simulations accurately captured the amount and spatial distribution of precipitation over the region, likely due to the complex topography and convective nature of the studied event. However, the WSM3 microphysics scheme and the use of ERA5 SST data provided slightly better representation of instability indices, although these configurations still underperformed in simulating the rainfall intensity. All simulations overestimated the instability indices compared to ERA5, although ERA5 itself may underestimate the convective environments. Despite some performance limitations, the sensitivity experiments provided valuable insights into the model's behavior under different configurations for southeastern Brazil—particularly in a convective environment within mountainous terrain. However, further evaluation across multiple events is recommended.

Keywords: extreme event; precipitation; sensitivity numerical experiments; WRF; southeast Brazil

check for updates

Academic Editors: Michael L. Kaplan and Anthony R. Lupo

Received: 27 March 2025
Revised: 29 April 2025
Accepted: 3 May 2025
Published: 5 May 2025

Citation: Garcia, D.W.; Reboita, M.S.; Carvalho, V.S.B. Sensitivity Analysis and Performance Evaluation of the WRF Model in Forecasting an Extreme Rainfall Event in Itajubá, Southeast Brazil. *Atmosphere* **2025**, *16*, 548. https://doi.org/10.3390/atmos16050548

Copyright: © 2025 by the authors. Licensee MDPI, Basel, Switzerland. This article is an open access article distributed under the terms and conditions of the Creative Commons Attribution (CC BY) license (https://creativecommons.org/licenses/by/4.0/).

1. Introduction

Extreme weather and climate events across the globe have become increasingly frequent and intense in recent years. Extreme weather events include short-term phenomena such as intense daily rainfall episodes, whereas extreme climate events refer to sequences of dry or wet days, for instance. According to the Intergovernmental Panel on Climate Change [1], extreme events are defined as those occurring rarely in a given location, falling within the upper or lower 10% of a probability distribution. These events can result in severe consequences, such as flooding and landslides [2–5], adverse health effects, including

waterborne diseases, psychosocial and behavioral disorders, cardiovascular diseases, and the exacerbation of chronic illnesses [6–8], as well as damage to infrastructure [9].

Several studies have reported an increasing trend in extreme precipitation events in Brazil, based on observational and reanalysis datasets [10–13] as well as satellite data [14]. Recent extreme rainfall events in Brazil include the 2020 and 2022 episodes in the Metropolitan Area of Belo Horizonte, Brumadinho, and Muriaé [15,16], and two extreme events in 2022 in Petrópolis [17–19]. Additionally, the highest recorded precipitation in Brazil in 24 h occurred on the northeastern coast of São Paulo in 2023 [20], with São Sebastião receiving approximately 683 mm in just 15 h [21]. According to the National Center for Monitoring and Early Warning of Natural Disasters [22], over 2000 people were left homeless, 2466 were displaced, and 70 fatalities were reported. The heavy rainfall triggered numerous landslides and flooding, which were the primary causes of fatalities in the affected areas [20]. More recently, an extreme rainfall event affected the northern and eastern region of the Rio Grande do Sul state between late April and early May 2024, leading to widespread flooding across the state [23,24].

In southeastern Brazil, the southern part of Minas Gerais (MG) state has been affected by extreme precipitation events multiple times, with the most severe cases registered in 1991 and 2000 [25]. Great amounts of precipitation typically occur between October and March, coinciding with the region's rainy season [26,27]. The municipality of Itajubá, located in southern Minas Gerais, is particularly vulnerable to such events, as shown by several climatological studies. For instance, Campos et al. [28] defined a threshold of 50 mm day^{-1} to identify extreme precipitation events in the city, recording 21 occurrences between 1998 and 2011. Among these, the 1–4 January 2000 event recorded daily rainfall exceeding 50 mm, with a total accumulation surpassing 180 mm, leading to the overflow of the Sapucaí River and significant disruptions to local communities [29].

On 27 February 2023, Itajubá and Pedralva municipalities were hit by a severe short-duration storm (approximately 40 min), resulting in extensive flooding, landslides, fallen trees, and structural damage. The event left 28 people homeless, including nine in Itajubá [30]. The storm also severely impacted the Federal University of Itajubá (UNIFEI), where rising water levels in a basin behind the campus caused flooding, leading to an estimated financial loss of approximately U$S 1,7 million due to damage to laboratories and structures [30]. At the time of the event, four rain gauges were operational in Itajubá—three managed by CEMADEN and one by UNIFEI (Figure 1). The university's meteorological station recorded 73 mm of rainfall. Approximately 2.5 km from UNIFEI, the Estiva neighborhood gauge, located near the city hall, recorded 58.8 mm, while the São Vicente gauge registered 43.8 mm, and the Sapucaí River station measured 24.6 mm over the 40-min period. Some damages caused by the storm in Itajubá on 27 February 2023 are shown in Figure 1.

Given the increasing frequency and intensity of extreme weather events, ensuring community safety depends on effective political management, which, in turn, relies on accurate meteorological monitoring and forecasting tools. To address this need, UNIFEI hosts the Center for Weather and Climate Forecasting Studies of Minas Gerais (CEPreMG), which operates daily numerical weather forecasts using version 4.4 of the Weather Research and Forecasting (WRF) model.

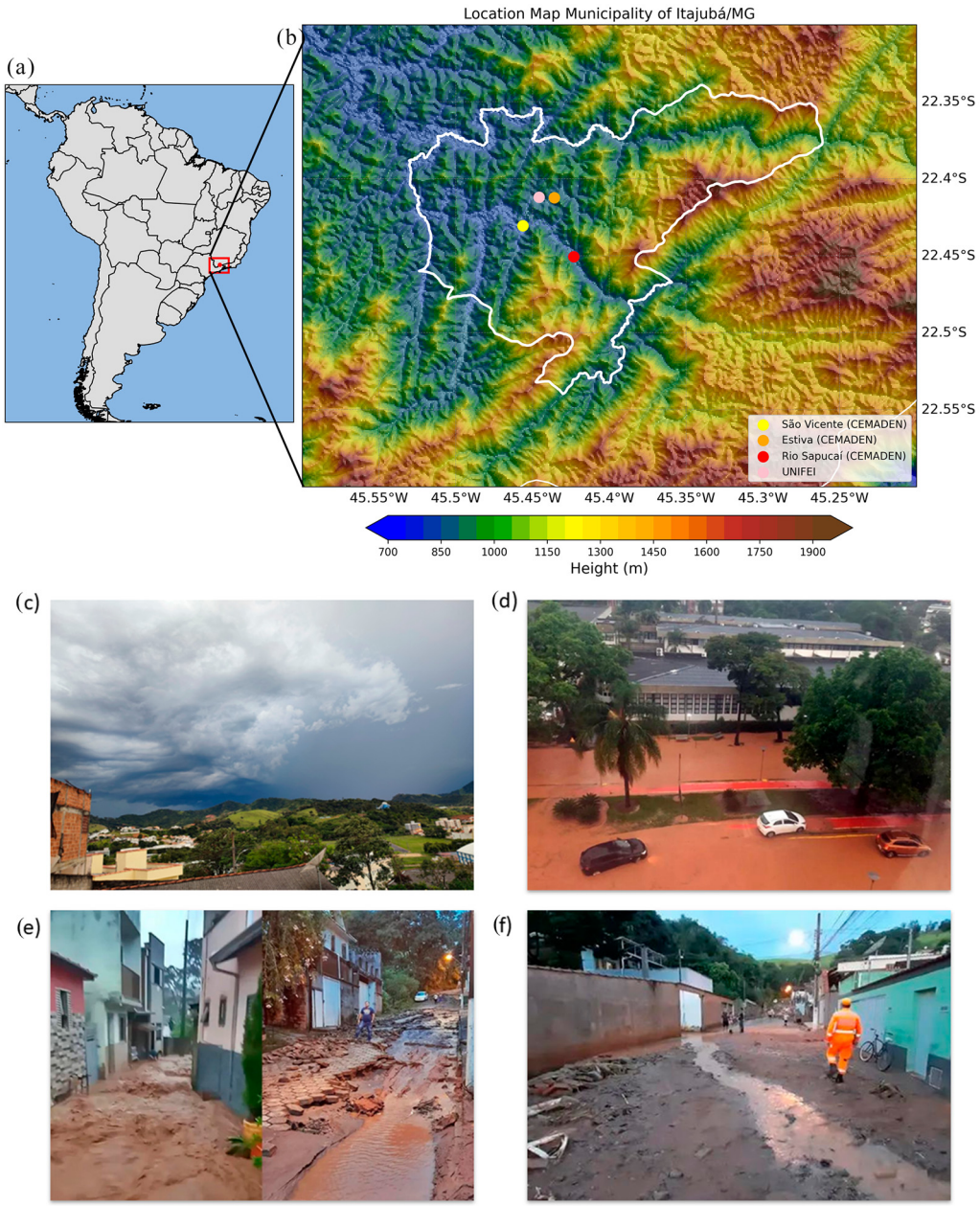


Figure 1. (**a**) Location of the study area (red box) in relation to South America; (**b**) topographic map (meters) of the municipality of Itajubá and the location of four rain gauge stations operating in the municipality as of February 2023 (topography was obtained from Shuttle Radar Topography Mission Global (SRTMGL3)); and (**c**–**f**) damages caused by the rainfall on 27 February 2023, more specifically, in (**c**) the storm, (**d**) flooding at the main entrance of the Federal University of Itajubá, (**e**) pavement detachment in Pedralva municipality, and (**f**) mud covering a street in the Anhumas neighborhood in Itajubá.

Since not all natural processes have equations for their simulation, numerical models require parameterizations to represent various physical processes, such as radiation, cloud microphysics, cumulus convection, and planetary boundary layer interactions. However, the choice of parameterization introduces uncertainties in simulations. For this reason, sensitivity experiments need to be performed to identify the best configuration for specific regions. Sensitivity studies using the WRF model in different regions of the world highlight, for instance, the crucial role of cloud microphysics parameterizations, with the Thompson and Morrison schemes yielding more accurate precipitation forecasts [31–34]. Experiments

analyzing the cumulus convection schemes indicate that the Grell–Freitas and Multi-Scale Kain–Fritsch (MKF) schemes perform best for mesoscale convective events, particularly in complex topographic regions, such as in southeastern Brazil [35,36]. Comparisons of initial and boundary conditions also suggest that the European Centre for Medium-Range Weather Forecasts Reanalysis v5 (ERA5) dataset improves WRF performance in simulating extreme precipitation, outperforming Global Forecast System (GFS) and Global Data Assimilation System (GDAS) due to its refined assimilation processes [37,38]. Therefore, sensitivity tests are essential to optimize the WRF configuration for both case studies and operational use.

In this context, the main goal of this study is to evaluate the performance of the WRF model in predicting the extreme precipitation event that affected the city of Itajubá on 27 February 2023 through sensitivity numerical experiments and to explore alternative model configurations that may enhance forecasting accuracy. Specifically, this study had the following aims: (1) characterize the atmospheric conditions associated with this extreme rainfall event and (2) assess the performance of different sensitivity numerical experiments, including (a) cloud microphysics parameterizations, (b) initial and boundary conditions, (c) sea surface temperature (SST), and (d) soil moisture.

2. Methodology

2.1. Study Area

The study area comprises the MG state (hereafter MG) in southeastern Brazil (Figure 1). Our major focus is on Itajubá municipality (22°30′30″ S–45°27′20″ W and 842 m above sea level) located in the Mantiqueira Mountain Range and hence characterized by a mountainous and rolling terrain and surrounded by the Atlantic Forest [39]. Southern MG, according to Köppen's classification, has a high-altitude tropical climate (hot and humid summers and cold, dry winters; [26]). However, the term "monsoon climate" is more commonly used to describe the climate features of this region. Itajubá, along with other cities in southern MG, experiences an average annual precipitation of approximately 1600 mm, with most of the rainfall concentrated in austral summer [26,40–45].

2.2. Data

2.2.1. ERA5 Reanalysis

The ERA5 reanalysis [46], from the European Centre for Medium-Range Weather Forecasts (ECMWF; https://climate.copernicus.eu/climate-reanalysis, accessed on 10 November 2024), provides meteorological variables at a spatial resolution of 0.25° and an hourly frequency; data availability has a latency of approximately five days. Variables used here include temperature, pressure, geopotential height, zonal and meridional wind components, and specific humidity at isobaric levels ranging from 1000 to 10 hPa. Additionally, mean sea level pressure, sea surface temperature, soil temperature, soil moisture, snow cover, accumulated precipitation, and terrain height were considered at surface level.

2.2.2. Global Data Assimilation System (GDAS) and Global Forecast System (GFS) Analyses

The GFS and GDAS models provide atmospheric analyses that are used as initial and boundary conditions in other numerical models. They have key differences in their data processing approaches [47]. GDAS requires a longer processing time as it integrates and analyzes observational data from various sources, such as satellites and meteorological stations, to generate an accurate initial dataset for numerical model initialization such as GFS. In contrast, GFS utilizes these initial conditions to rapidly produce forecasts without direct assimilation of observational data, enabling the quick dissemination of weather predictions to meet various sector demands. These datasets are publicly available at

https://www.ncei.noaa.gov/products/weather-climate-models/global-forecast (accessed on 12 November 2024). GDAS and GFS data have a spatial resolution of 0.25° and are provided at standard synoptic times (0000, 0600, 1200, and 1800 UTC). Forecasts extend up to 72 h, with simulations initialized 24 h before the reference time.

2.2.3. Radar Data

The Centro Tecnológico de Hidráulica Foundation (FCTH; https://www.saisp.br/estaticos/sitenovo/produtos.html, accessed on 1 December 2024) provides radar data, which is installed at the Ponte Nova dam, located at the headwaters of the Tietê River (23.59° S, 45.97° W). The radar operates in the S-band, with a range of 240 km and a frequency of five minutes. From the radar, Constant Altitude Plan Position Indicator (CAPPI) products and radar-based precipitation estimates are used in this study. The city of Itajubá, approximately 140 km from the radar, is within its coverage area, allowing for crucial insights into storm movement, reflectivity, and internal structure.

The CAPPI provides storm cloud reflectivity at constant altitudes, allowing for a detailed examination of storm cell internal structure, detecting water, supercooled water, graupel, ice, etc. [48]. In addition, it allows the classification of the precipitation in stratiform or convective [49,50]. For this classification, thresholds are used to distinguish between areas of intense convective updrafts and widespread stratiform precipitation [51].

2.2.4. Geostationary Operational Environmental Satellite (GOES) Data

Geostationary Operational Environmental Satellite 16 (GOES-16) is a geostationary satellite launched in 2016 by the American agencies, National Oceanic and Atmospheric Administration (NOAA) and National Aeronautics and Space Administration (NASA). It features 16 spectral channels, including 2 visible channels, 4 near-infrared channels, and 10 infrared channels. The spatial resolution of each channel ranges from 500 m to 2 km, with a temporal resolution of 10 min. The data used in this study were obtained from GOES-16′s Channel 13 (infrared, 10.3 μm) and are available at: https://noaa-goes16.s3.amazonaws.com/index.html (accessed on 12 November 2024).

2.2.5. Precipitation Measurements

Precipitation data were obtained from different sources as follows:

- In situ data: Hourly precipitation data from 60 rain gauges and weather stations, located in the states of MG and São Paulo (SP), were provided by CEMADEN (http://www2.cemaden.gov.br/mapainterativo/, accessed on 15 November 2024) and the National Institute of Meteorology (INMET, https://portal.inmet.gov.br/, accessed on 15 November 2024). The stations are spread across the municipalities of Itajubá, Lambari, Juiz de Fora, Passos, Poços de Caldas, Extrema, Santa Rita do Sapucaí, São Lourenço, and Maria da Fé in MG and Lorena, Campos do Jordão, Cachoeira Paulista, São Bento do Sapucaí, and Atibaia in SP.
- Gridded datasets: Gridded precipitation was provided by the MERGE/CPTEC and Rainfall Estimates from Rain Gauge and Satellite Observations (CHIRPS). The MERGE/CPTEC combines data from the Global Precipitation Measurement (GPM) Integrated Multi-satellite Retrievals for GPM (IMERG) [52,53] with ground-based observations. The MERGE/CPTEC dataset has a spatial resolution of 0.1° (~10 km), frequency of 30 min, and is available at http://ftp.cptec.inpe.br/modelos/tempo/MERGE/GPM (accessed on 15 November 2024).

The CHIRPS dataset merges precipitation estimates from the Climate Hazards Group Infrared Precipitation (CHIRP) with in situ meteorological station observations. This product offers a spatial resolution of 0.05° and features a long historical record, span-

ning from 1981 to the present [54]. CHIRPS provides precipitation data at different temporal scales, including daily (used in this study), monthly, annual, and pentadal (five-day) averages. This dataset is available at https://www.chc.ucsb.edu/data/chirps (accessed on 15 November 2024).

2.3. WRF Model

The WRF model [55,56], developed by the National Oceanic and Atmospheric Administration/National Centers for Environmental Prediction (NOAA/NCEP), is a widely used numerical model for mesoscale weather forecasting and atmospheric case studies. One of WRF's strengths is its modular physics structure, which offers a wide range of physical parameterization schemes—including options for microphysics, cumulus convection, planetary boundary layer processes, surface layer physics, land surface models, and radiation schemes. Specifically, WRF version 4.4, used in this study, includes 22 microphysics parameterization schemes that represent cloud and precipitation processes with varying degrees of complexity. A detailed list of these schemes is available at https://www2.mmm.ucar.edu/wrf/users/physics/phys_references.html#CU (accessed on 10 September 2024).

In this study, we adopt the same WRF configuration used in the CEPreMG. The model setup consists of two nested domains with horizontal resolutions of 12 km (D-01) and 3 km (D-02), as shown in Figure 2. Forecasts are produced up to 72 h in advance; however, the first 12 h are excluded from the analysis to account for the model spin-up period, which allows for dynamic and thermodynamic adjustment [34,56–59]. The inner 3 km domain is particularly well suited for resolving local orographic circulations—such as mountain–valley breeze systems—that frequently influence extreme precipitation events in southeastern Brazil, as demonstrated by previous studies [59,60].

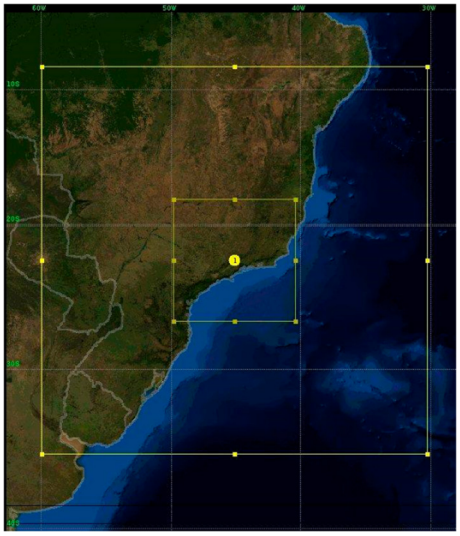


Figure 2. Nested grids of the WRF model used at CEPreMG and in this study, with the outer grid (D-01) having a spatial resolution of 12 km and the inner grid (D-02) at 3 km. The grids are centered at 45.45°W and 22.45°S, indicated by number 1, corresponding to the municipality of Itajubá.

The WRF model was initialized and forced at the lateral boundaries using the GFS data, which have a horizontal resolution of 0.25° × 0.25° latitude–longitude and a frequency of 6 h. Additional configuration details are available in Table 1. By default, WRF incorporates land cover, sea surface temperature (SST), and soil moisture data from the Terra and Aqua satellites' Moderate Resolution Imaging Spectroradiometer (MODIS) Land Cover Type (MCD12Q1).

Table 1. WRF model configurations used for weather forecasting simulations at CEPreMG and in this study, except for sensitivity experiments where physical parameterizations were modified.

Parameter	Outer Domain (D01)	Inner Domain (D02)
Points in X-direction	190	153
Points in Y-direction	240	181
Points in Z-direction	42	42
Horizontal Resolution	12 km	3 km
Timestep	60	15
Central Latitude	22.4255° S	
Central Longitude	45.4527° W	
Cumulus Convection	Grell–Freitas [61] This option is turned off for D-2 grid.	
Microphysics	WSM3 [62]	
Planetary Boundary Layer	Yonsei University Scheme [63]	
Surface Layer	Revised-MM5 [64]	
Land-Surface	Noah-LSM [65]	
Shortwave Radiation	MM5 [66]	
Longwave Radiation	RRTM [67]	

2.4. Design of the Sensitivity Numerical Experiments

To assess the performance of the WRF model in simulating the extreme precipitation event that occurred in Itajubá on 27 February 2023, a series of sensitivity numerical experiments were conducted (Table 2). The control simulation followed the same configuration operationally adopted by CEPreMG (described in Table 1), while additional sensitivity experiments were designed to evaluate the influence of different physical parameterizations, boundary conditions, and surface characteristics (Table 2).

The first set of experiments focused on microphysics schemes comparing the WSM3 (default configuration at CEPreMG), WSM6, and WDM6 schemes. While WRF Single-Moment 3-class (WSM3, [55,62,66,68]) uses a simplified approach with three hydrometeor classes, WRF Single-Moment 6-class (WSM6, [62,69,70]) incorporates six classes, enhancing the representation of mixed-phase processes. The WRF Double-Moment 6-class (WDM6, [68,70]) scheme extends WSM6 by introducing prognostic equations for cloud droplet and rainwater number concentration, offering a more detailed treatment of precipitation microphysics. Although WRF offers 22 microphysics parameterization schemes, we focus on evaluating WSM3, WSM6, and WDM6 in this study for the following reasons: WSM3 is the default configuration used in CEPreMG's operational forecasts, and we aim to compare the performance of alternative schemes relative to this baseline. WSM6 represents an extended version of WSM3 and warrants further analysis. WDM6 was identified by [33,58] as showing slightly better skill in representing both warm-rain and mixed-phase processes based on a broader sensitivity analysis that included Thompson, Milbrandt 2-moment, Morrison 2-moment, and WDM6 schemes.

Another key aspect analyzed was the impact of different initial and boundary conditions, replacing the default GFS data with GDAS and ERA5 reanalysis. In addition, experiments examined the role of surface conditions, specifically sea surface temperature (SST) and soil moisture. The default WRF configuration relies on climatological SST and soil moisture data, but alternative simulations tested weekly ERA5 SST and GDAS soil moisture

datasets, aiming to assess whether real-time variations in surface conditions enhance model performance.

Table 2. Sensitivity numerical experiments.

Experiments	Description
WSM3	WRF CEPreMG control configuration, using the WSM3 microphysics scheme, GFS initial and boundary conditions, SST, and climatological soil moisture.
WSM6	Change in the microphysical parameter, using the WSM6 microphysics scheme, which is a system that has six classes instead of three, used by CEPreMG.
WDM6	Change in microphysical parameter, using WDM6 microphysics scheme, which takes into account mass and particle quantity.
GDAS	The initial and boundary condition is GDAS.
ERA5	The initial and boundary condition is ERA5.
SST	Change in climatological SST, the standard used in the model, by weekly SST. The same is used by ERA5 data.
SOIL	Soil moisture changes with climatological data, standard used in the model, by weekly soil moisture. Same used by GDAS data
ERA5_SST	Simulation with the best results obtained from previous simulations. In this case, the initial and boundary conditions data and the SST data were changed from climatological to weekly.

Following the identification of the best-performing configurations from each sensitivity category, a final simulation, ERA5_SST, was performed, integrating ERA5 boundary conditions with weekly SST data to optimize accuracy.

2.5. Analyses

The extreme precipitation event that occurred on 27 February 2023 in Itajubá, MG, was analyzed using a combination of radar data, which provides a mesoscale perspective of the storm and synoptic-scale diagnostics. The temporal evolution of precipitation was examined through radar reflectivity data, allowing for the classification of precipitation into convective and stratiform regimes [51] as well as the distinction between severe and non-severe storms [50]. Additionally, the atmospheric conditions that contributed to the development of the extreme event were characterized, offering insights into the dynamical and thermodynamical processes responsible for the observed precipitation.

The performance of the sensitivity numerical experiments (Table 2) was evaluated through an analysis of the following parameters:

(a) The precipitation spatial pattern: simulated hourly precipitation was compared with CHIRPS, MERGE, and ERA5 datasets;

(b) Statistical measurements: bias, Pearson correlation coefficient, and Kling–Gupta efficiency (KGE, which measures overall agreement between model outputs and observations [71]) were computed between the hourly model and ERA5 precipitation data;

(c) Atmospheric instability indices: To determine the performance of the sensitivity numerical experiments in simulating the atmospheric conditions conducive to convection and severe weather [72], we compared thermodynamic instability indices—K [73], Total Totals (TT; [74]), and Convective Available Potential Energy (CAPE; [49]) simulated and

from ERA5. The indices were calculated with the basic variables provided by the model and ERA5. We did not use the indices available in these datasets in order to keep the consistency in the methodologies used to obtain them. In addition, we analyzed vertical wind shear between 500 and 1000 hPa. The equations used to calculate the indices, along with the threshold values indicative of the associated atmospheric conditions, are provided in the Supplementary Material.

3. Results and Discussion

3.1. Characterization of the Study Case

Figure 3 depicts the time–space evolution of the storm over Itajubá, showing precipitation rate estimates obtained from radar between 1900 and 1955 UTC. The rainband moves from northwest to southeast, with precipitation rates exceeding 80 mm h^{-1}, which is classified as heavy rainfall when exceeding 50 mm h^{-1} [75].

Reflectivity analysis indicated values exceeding 55 dBZ over the central region of Itajubá (Figure 4a), coinciding with the location of rain gauges that recorded high precipitation totals, including the UNIFEI station, where precipitation reached 73 mm. Values exceeding 55 dBZ are recognized as a threshold for hail detection [48]. As the rainband was intense and included hail, these features classified the storm as severe [50]. The storm also exhibited significant vertical development, with cloud tops exceeding 14 km in altitude, while reflectivity values within the storm ranged between 30 and 40 dBZ (Figure 4b).

Radar data also allow for the classification of storms as stratiform (reflectivity below 30 dBZ) or convective (reflectivity above 30 dBZ) [50]. Figure 4c shows that reflectivity values exceed 30 dBZ over a large portion of Itajubá, indicating that the storm was convective. Convective storms are characterized by intense precipitation over short periods (here it was ~40 min) and are often associated with hail formation. The great amount of rainfall produced by this type of cloud was confirmed by precipitation measurements from Itajubá (Figure 5). As the Rio Sapucaí station is southeast of the other stations (Figure 1), the peak of precipitation occurred later (Figure 5), which is consistent with the storm's displacement (Figure 3).

Several key ingredients are required for storm development: moisture availability, an air-lifting mechanism, atmospheric instability, and the presence of vertical wind shear between 6 km and the surface (typically approximated by the 500 hPa and 1000 hPa pressure levels) [76–78]. The synoptic scale helps identify moisture sources and dynamic mechanisms that drive air ascent while also providing a broad assessment of CAPE (a proxy for atmospheric instability) and vertical wind shear.

To understand the storm's precursor environment, the atmospheric variables need to be analyzed at different time steps throughout the day and prior to the storm's occurrence. Hence, Figure 6 depicts the evolution of different synoptic-scale fields on 27 February 2023 at 1200 and 1800 UTC. At these times, a frontal system was present near southern Brazil, connecting to a low-pressure center over the Atlantic Ocean, without any influence in the study area. The dominant feature in the study area (southern MG; Figure 6) was a lack of large-scale dynamic forcing for upward movement (i.e., frontal system, upper-level jet streaks, and/or mid-level troughs). On the other hand, relative humidity at 850 hPa exceeded 80% in southern MG (Figure 6e,f), suggesting a moist boundary layer. Indeed, in this region, the convergence of the vertically integrated moisture flux was predominant, although it was not associated with strong large-scale circulation patterns (Figure 6i,j).

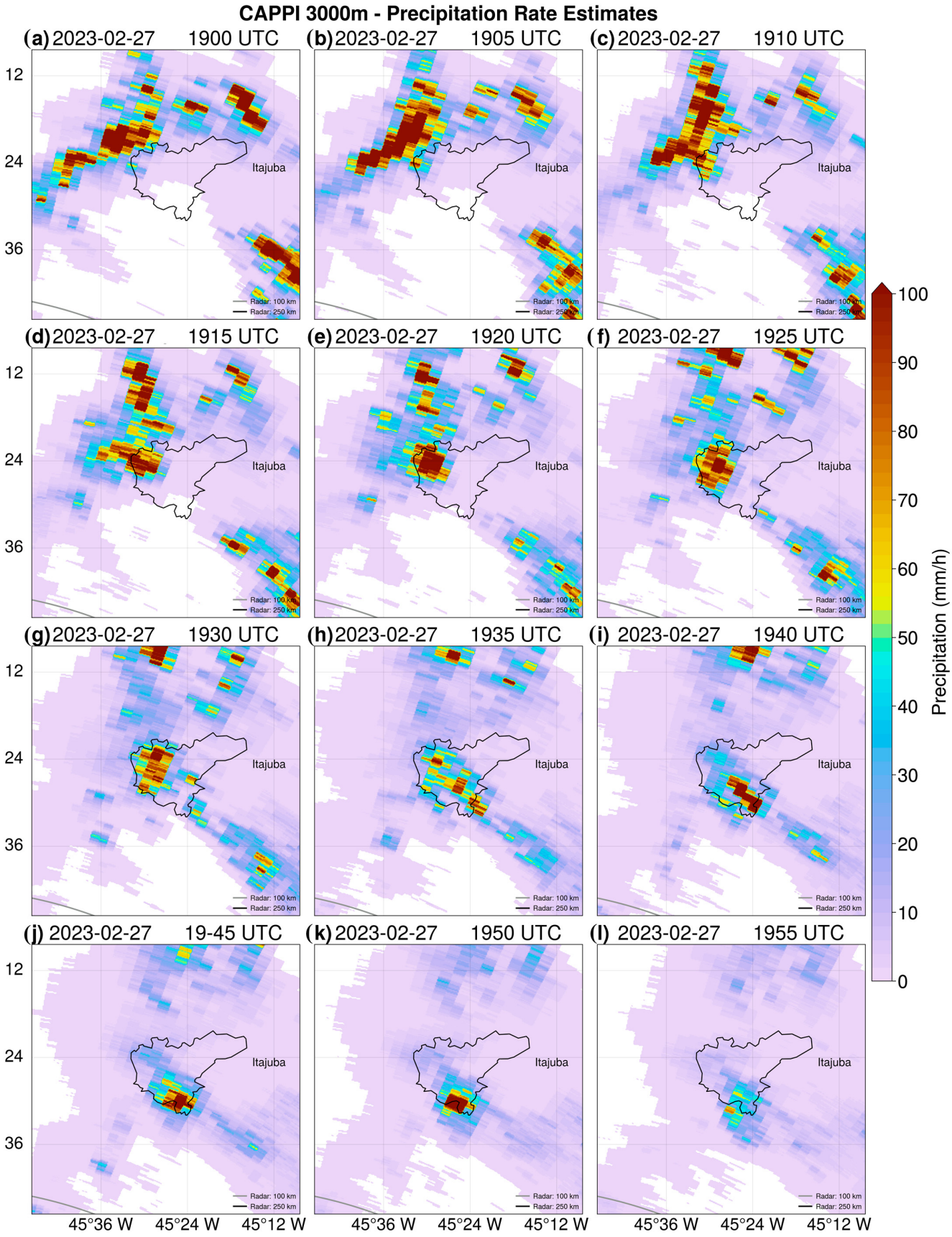


Figure 3. Precipitation rate estimates (mm/h) derived from the ZDR relationship applied to FCTH radar data at different time intervals between (**a**) 1900 UTC and (**l**) 1955 UTC on 27 February 2023.

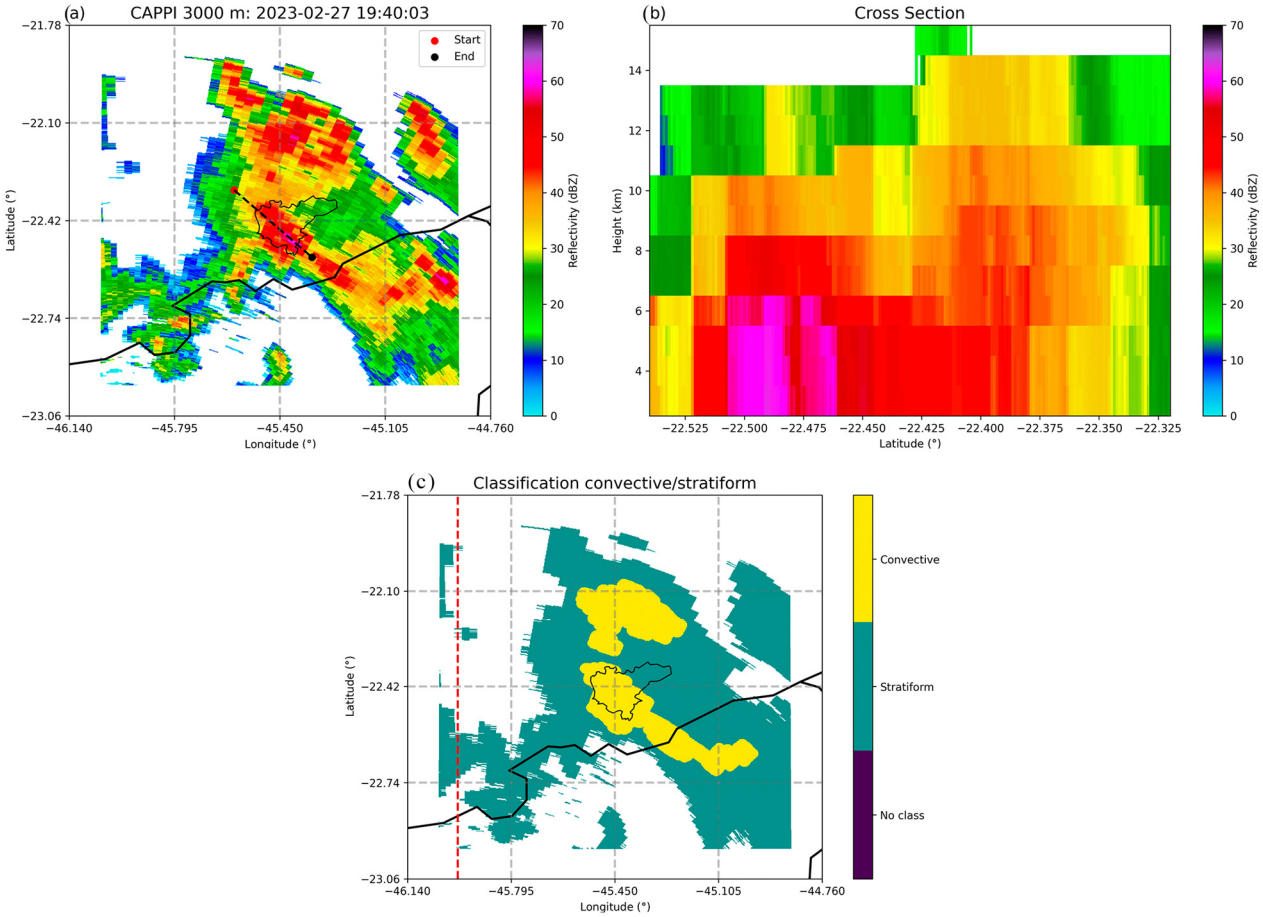


Figure 4. CAPPI of radar reflectivity from FCTH at an altitude of 3 km. (**a**) CAPPI at 1940 UTC, (**b**) cross-section of the CAPPI at 1940 UTC along the path indicated by the line in panel (**a**), (**c**) convective/stratiform classification of the storm at 1940 UTC on 27 February 2023.

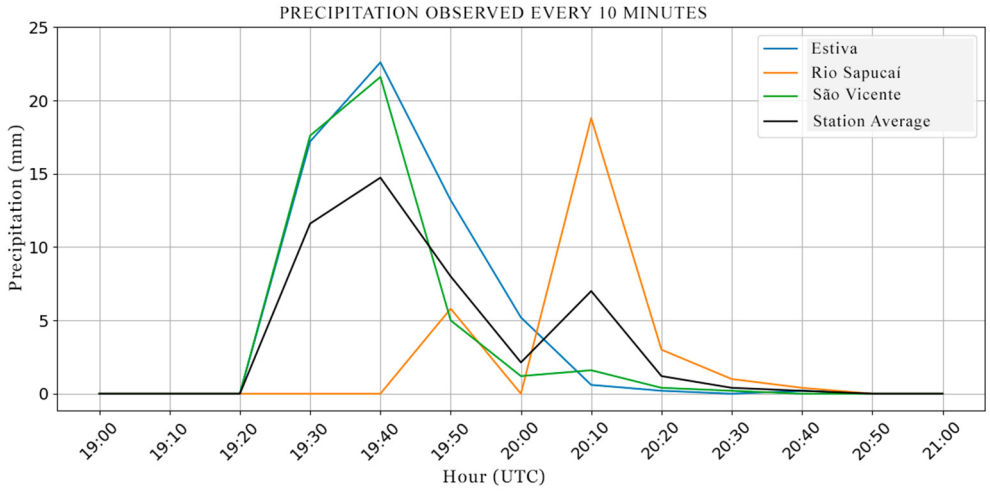


Figure 5. Precipitation (mm) recorded every 10 min by CEMADEN rain gauges in the municipality of Itajubá: Estiva (blue), Rio Sapucaí (orange), São Vicente (green), and the average of the stations (black) on 27 February 2023. Data from the UNIFEI station were not plotted because the station was recording only daily totals during that period.

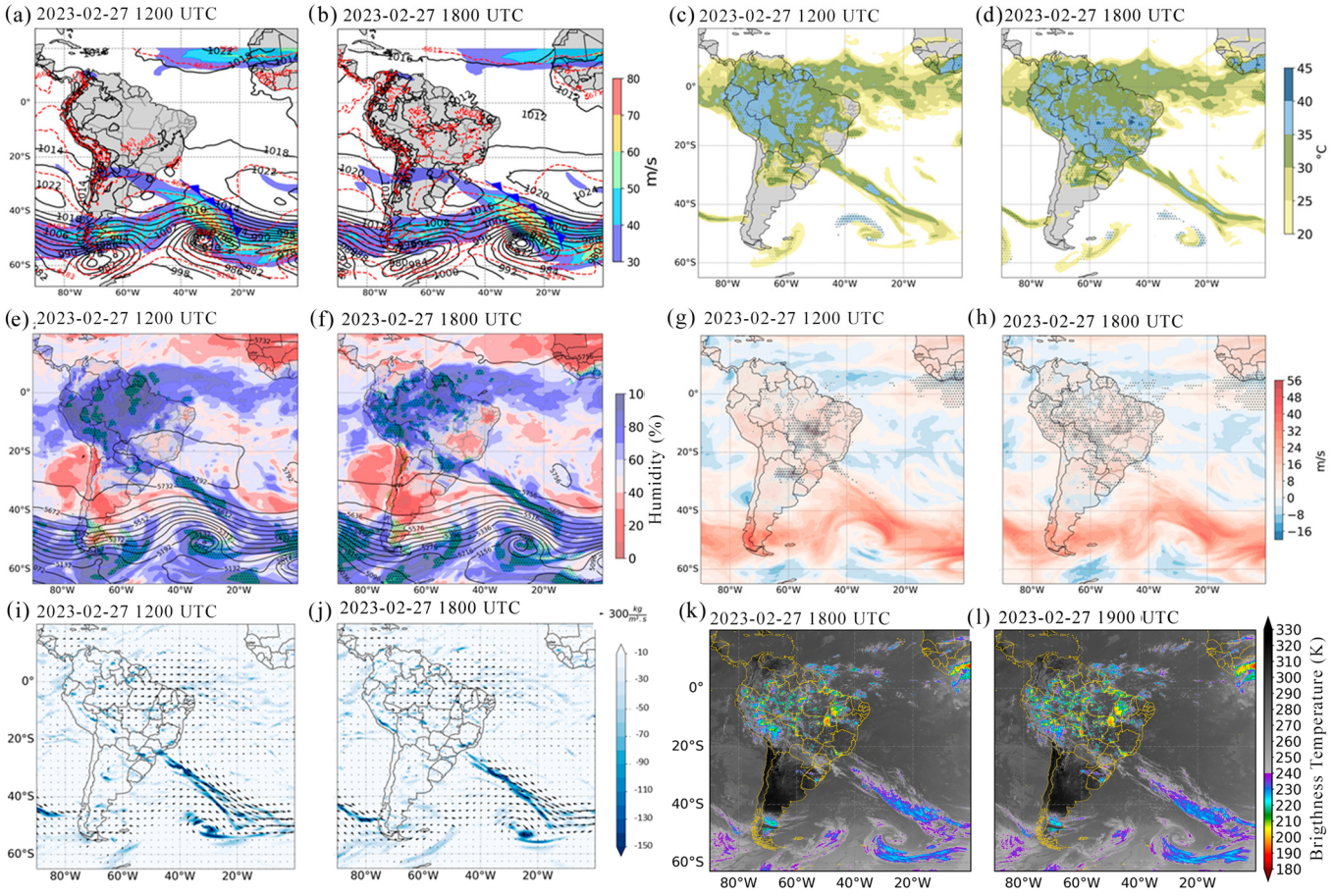


Figure 6. Synoptic fields for 27 February 2023 at 1200 and 1800 UTC. (**a**,**b**) Mean sea level pressure (hPa, solid black lines), 250 hPa winds with speeds exceeding 30 m s^{-1} (shaded), and 500–1000 hPa thickness (m, red dashed lines); (**c**,**d**) Total Totals Index (°C, dashed for values above 45 °C) and K Index (°C, shaded); (**e**,**f**) relative humidity at 850 hPa (%, shaded), 500 hPa geopotential height (m, solid black lines), and 500 hPa vertical motion (Pa s^{-1}, dashed); (**g**,**h**) vertical wind shear between 500 and 1000 hPa (m s^{-1}, shaded) and CAPE (J kg^{-1}, dashed for values above 500 J kg^{-1}); (**i**,**j**) convergence of the vertically integrated moisture flux (between 1000 and 100 hPa (kg m s^{-1}, shaded) and flux vectors (kg m^{-2} s^{-1} black arrows); and (**k**,**l**) brightness temperature (K) from GOES-16, channel 13 (10.3 µm), but to 1800 and 1900 UTC. In all panels, the red box indicates the southern part of MG.

The combination of moisture and convergence contributed to the formation of cloud cover, represented in Figure 6k,l by brightness temperature data from GOES-16. A small cluster of clouds with very cold tops was observed along the SP–MG border, while the frontal system over the ocean exhibited warmer cloud tops, indicating a less intense convective structure compared to the cloud cover over the continent.

At the mesoscale, the primary factor contributing to upward motion appears to be diurnal heating. According to UNIFEI's meteorological station, the maximum temperature recorded on February 27 was 31.4 °C. The combination of high surface temperature and moisture flux convergence (Figure 6i,j) in the region were the ingredients to cloud formation. Indeed, Figure 6f shows upward motion (negative omega) at 500 hPa over the Mantiqueira mountain range, between the states of MG and SP, further supporting the role of surface heating in triggering convection.

Atmospheric instability is further indicated by thermodynamic indices such as Total Totals (TT), K-index, and CAPE (Figure 6c,d,g,h). In southern MG, the K-index exceeded 30 °C (Figure 6c,d), suggesting favorable conditions for isolated thunderstorms [73], while

TT values were above 45 °C (Figure 6c,d), indicating the possibility of storms. A strong indicator of storm sustainability and organization is the presence of both vertical wind shear and CAPE, as vertical wind shear prevents the updrafts and downdrafts from canceling each other within the storm, allowing for storm intensification and longer duration. CAPE is an indicator of ascendant movement and instability. However, not all storms exhibit these two drivers. It was the case of the studied storm (Figure 6g,h). In southern MG, vertical wind shear was very low (4.82 m s^{-1}), while CAPE values reached 1023 J kg^{-1}. According to [72], CAPE values exceeding 1000 J kg^{-1} indicate a moderately unstable atmosphere, with a significant probability of thunderstorm development. These results indicate that the thermodynamic conditions were enough to support the storm development [79].

3.2. Numerical Experiments

3.2.1. Precipitation

Figure 7 presents the daily accumulated precipitation on 27 February 2023, derived from weather stations (observations), ERA5 reanalysis, satellite-based estimates (CHIRPS and MERGE), and WRF model experiment results (as detailed in the methodology). The analysis focuses solely on the simulations with a 3 km grid, which provide the highest horizontal resolution.

Meteorological stations (Figure 7a) indicated that on February 27, the city of Itajubá recorded 59,1 mm of precipitation (average from three stations managed by CEMADEN and one by UNIFEI in the studied region). Other nearby cities, such as Lambari, Maria da Fé, and São Lourenço, also recorded rainfall on the same day. ERA5 (Figure 7b) does not indicate precipitation over the studied region, only shows it near the MG–SP border, and does not exceed 25 mm. Its coarse spatial resolution of 0.25° may have contributed to the underestimation of precipitation. On the other hand, CHIRPS (Figure 7c), with a higher horizontal resolution (0.05°), registered precipitation values between 40 and 45 mm in areas close to Itajubá. Additionally, CHIRPS indicates precipitation in other parts of southern MG, the Paraíba Valley, and a small portion of the SP state coastline, aligning with areas that recorded rainfall on February 27. MERGE (Figure 7d) also does not represent precipitation over southern MG and the Paraíba Valley as effectively as CHIRPS. The highest rainfall volumes in MERGE were concentrated over the Atlantic Ocean (100 mm), while a small isolated region in southern MG, near Itajubá, showed values close to 30 mm. In a nutshell, CHIRPS is the grid dataset more similar to the observations.

Comparing the simulations with observations and CHIRPS, we can see that the control simulation did not accurately represent the precipitation in southern MG (Figure 7e). The highest rainfall volumes were concentrated in the southern SP state, whereas in the region of interest, values were lower than those recorded by meteorological stations. According to the CHIRPS, MERGE, and ERA5 data, rainfall occurred in regions near the SP–MG border. However, none of the experiments properly captured the spatial pattern (Figure 7e–l), likely due to the region's complex topography and the representation of the vertical distribution of hydrometeors by microphysical parameterization schemes [33,80]. The accurate representation of terrain plays a crucial role in simulating precipitation patterns, as it directly influences orographic enhancement, rain shadow effects, and local wind patterns, which are particularly relevant in regions with significant elevation variations [81]. Inadequacies in resolving these topographic influences may have contributed to discrepancies in the spatial distribution of precipitation in the simulations.

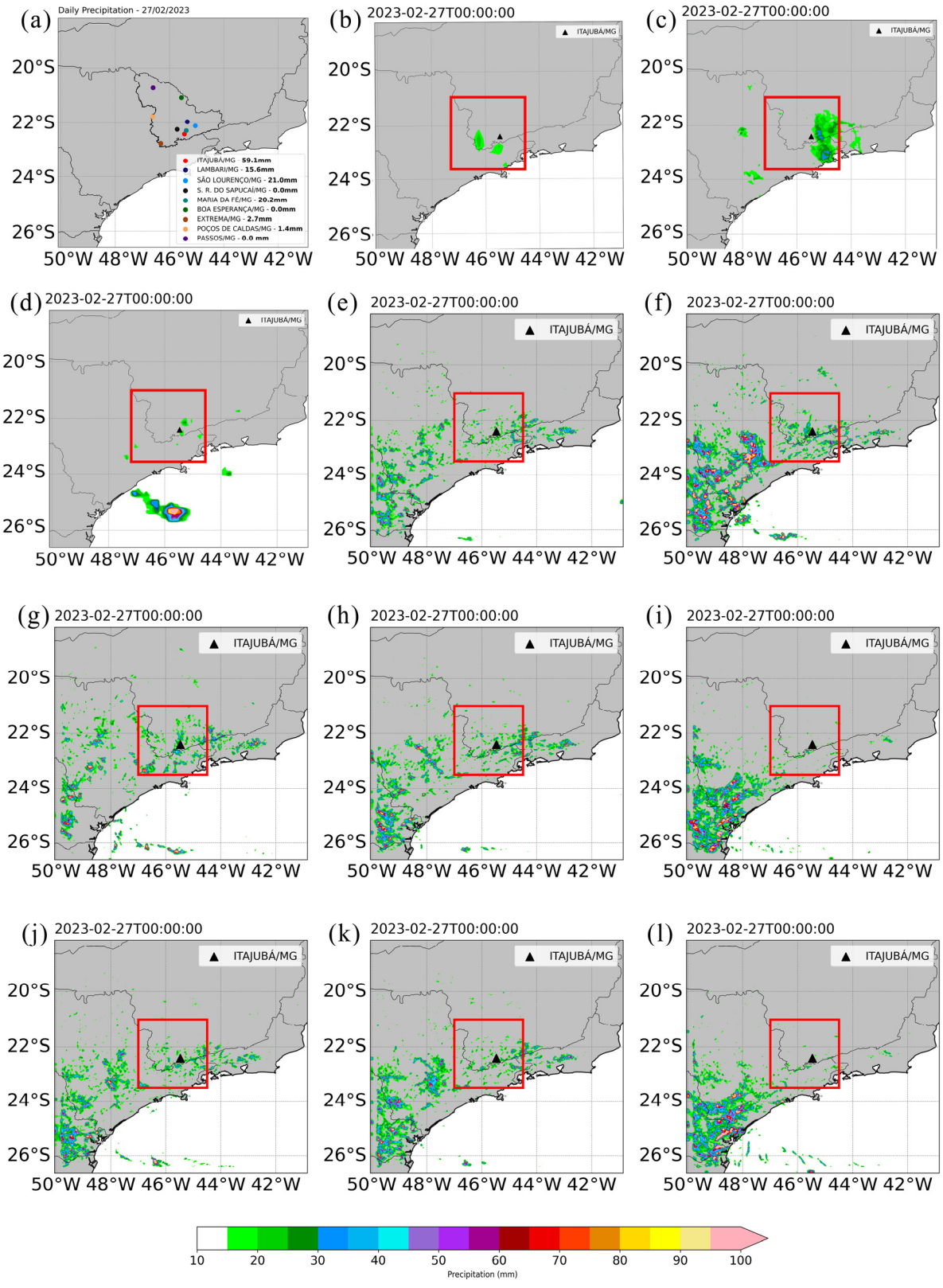


Figure 7. Daily accumulated precipitation (mm, shaded) for 27 February 2023 using different data sources and simulations: (**a**) meteorological stations (average of the stations of each city), (**b**) ERA5 reanalysis, (**c**) CHIRPS, (**d**) MERGE, (**e**) WSM3 (control), (**f**) WSM6, (**g**) WDM6, (**h**) GDAS, (**i**) experiment with ERA5 data, (**j**) SST, (**k**) SOIL, (**l**) ERA5_SST. The red box indicates the southern part of MG and northeast SP, and black triangle highlights the municipality of Itajubá.

We also analyzed the performance of the WRF sensitivity experiments in Itajubá using statistical indices (Table 3), with the average hourly precipitation recorded by the three CEMADEN stations as a reference (UNIFEI station data were not included due to the absence of hourly records). We extracted from each simulation the time series corresponding to the locations of each of the three CEMADEN stations. However, instead of selecting only one grid point per time step, we used the average of the nine closest grid points to the desired location.

Table 3. Statistical results of the WRF numerical experiments for Itajubá considering the hourly time series. KGE and Pearson correlation (R) were computed from February 26 at 1200 UTC to 28 at 0000 UTC, and the bias was computed just for the event day (February 27).

	Experiments	KGE	R	Bias
Microphysics	WSM3	−0.34	0.14	−31.3
	WSM6	−0.27	0.32	−37.6
	WDM6	−0.07	0.15	−35.9
Initial and boundary conditions	GDAS	−0.46	0.15	−39.0
	ERA5	−0.67	−0.03	−42.1
Boundary conditions	SST	−0.26	0.11	−41.3
	SOIL	−0.49	0.01	−37.7
	ERA5_SST	−0.57	0.19	−43.3

Figure 8a shows the average hourly precipitation observed in Itajubá and that from the experiments, as well as the simulation biases. There is a model precipitation underestimation in Itajubá, with consistently negative bias across all experiments (Figure 8b). Among the microphysics experiments, WSM3 presented the lowest bias (−31.3 mm), although all schemes underestimated precipitation. (Table 3). The adoption of soil moisture and sea surface temperature conditions from ERA5 and GDAS also did not bring substantial improvements to the city's precipitation simulation. This suggests that although the model's default configuration is not ideal, it remained competitive compared to the alternative configurations tested.

The KGE index values were predominantly negative across all experiments, indicating an unsatisfactory performance in reproducing the precipitation patterns (Table 3). The model's default configuration (WSM3) resulted in a KGE of −0.34 and a correlation of 0.14, while the WDM6 microphysics scheme showed a slight improvement in statistical efficiency, achieving a KGE of −0.07, although with a similarly low correlation (0.15). Moreover, initial and boundary conditions based on ERA5 reanalysis did not yield significant improvements for the city, presenting an even lower KGE (−0.67) and an almost null correlation (−0.03).

We also present in Figure 8c,d a comparison of the simulated hourly time series with the observed data, considering the average precipitation in the south of MG (cities shown in Figure 7a). Despite differences in the precipitation amounts, it is important to highlight that all simulations were able to represent the afternoon timing of precipitation during the analyzed period.

The diversity of sensitivity numerical experiments revealed additional underlying issues that must be investigated to enhance the model's performance in predicting precipitation. It is also important to note that although convection is explicitly resolved on a 3 km grid, other parameterization schemes remain essential, particularly for cloud microphysics. These schemes govern the formation, growth, and fallout of hydrometeors, directly influ-

encing precipitation processes. Fine-tuning the microphysics parameterization may help improve the accuracy of precipitation simulations and should be a focus of future studies.

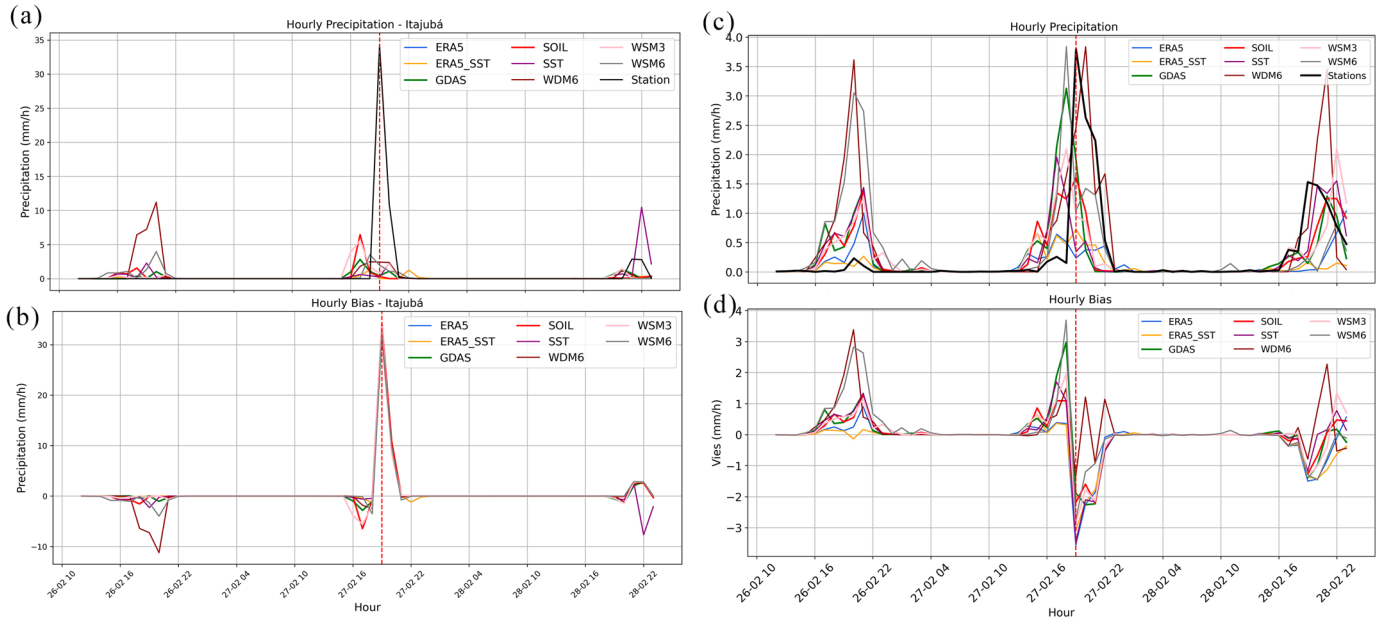


Figure 8. (**a**) Hourly precipitation (mm hour^{-1}) and (**b**) hourly bias for the 3 km grid in Itajubá between 26 and 28 February 2023. The simulations are as follows: WSM3 (red), WSM6 (green), WDM6 (blue), and the CEMADEN station data average (black). UNIFEI station was not included due to the absence of hourly data. (**c**,**d**) are similar to (**a**,**b**), but considering the average of the cities (Figure 7a) in the south of MG. In all panels, the dashed line indicates the time of heavy precipitation.

Unlike temperature and wind, which are governed by prognostic equations in numerical models, precipitation relies heavily on parameterizations for accurate forecasting. Therefore, a comprehensive understanding of the atmospheric environment requires the use of proxies such as instability indices. The following section focuses on these indicators and their relevance to the precipitation event under study.

3.2.2. Atmospheric Instability Indices

Instability indices are widely used as indicators of atmospheric conditions favorable for storm formation [72,82,83]. However, relying on a single index may be insufficient to fully characterize the atmospheric state and, in some cases, may not accurately represent conditions in specific regions. Therefore, combining multiple indices offers a more comprehensive understanding of the atmospheric instability. Indeed, weather forecasters rely on their expertise along with various precipitation proxies rather than solely on simulated precipitation to issue their forecasts. It is also important to emphasize that the ingredients necessary for storm development should be assessed prior to the event rather than at the exact time of occurrence. Thus, this study presents the simulated instability indices for 27 February 2023 at 1800 UTC.

Figure 9 displays the TT and K indices at 1800 UTC, one hour prior to the event in Itajubá, while Figure 10 presents CAPE exceeding 500 J kg^{-1} and vertical wind shear between 500 and 1000 hPa. In addition, we show Table 4 that summarizes these variables for Itajubá. Over southern MG (the region indicated by the red box), TT values exceed 44 °C in both ERA5 and experiments, while the K index ranges between 30 and 35 °C in ERA5 and around 40–45 °C in the simulations (Figure 9; Table 4). Both indices in ERA5 and the experiments indicate potential for thunderstorms [72,84]. According to Table 4, the K index from the ERA5 reanalysis classifies the environment as supporting scattered

thunderstorms, and only one simulation fell within this classification: the WSM3 experiment. Meanwhile, the TT index classified the conditions as weak thunderstorms, and the WSM6 experiment was the only one that classified it as moderate thunderstorms, while the remaining simulations correctly classified the index. The classification was based on thresholds by [73] for K and [74] for the TT index, and the simulations were considered accurate if they reproduced the correct classification category, even with different absolute values.

Table 4. Average of the atmospheric fields from ERA5 and simulated by WRF for Itajubá at 1800 UTC on 27 February 2023.

Experiments	CAPE	Wind Shear	K	TT	Daily Rainfall
ERA5	1023.2	4.82	32.9	45.2	5.9
WSM3	537.0	0.64	33.8	46.8	14.1
WSM6	1387.4	0.20	39.9	49.2	7.7
WDM6	254.5	2.23	40.2	47.7	9.4
GDAS	163.5	1.66	35.6	47.3	6.3
ERA5 (WRF)	1554.0	0.64	36.5	47.3	3.3
SST	1033.1	0.57	36.4	47.8	4.1
SOIL	439.2	0.02	39.1	48.1	7.7
ERA_SST	1994.5	0.68	37.5	48.3	2.0

A CAPE higher than 500 J kg^{-1} appears in ERA5 as a band extending from the northwest to the southeast along the MG–SP border (Figure 10a), while in the experiments, this variable is simulated across the entire displayed area in Figure 10, indicating more unstable conditions. Focusing on the Itajubá area (Table 4), ERA5 indicates a CAPE of 1023.2 J kg^{-1}, suggesting a moderately unstable atmosphere [71], and the simulation that most closely matched this value is the one with modified SST input data, which predicted a CAPE of 1033.1 J kg^{-1}. Although higher CAPE values were simulated in some experiments (e.g., ERA5_SST), this did not translate to increased precipitation. This reinforces the idea that high thermodynamic potential alone was not sufficient for rainfall realism in the WRF simulations of this event.

In general, the experiments tend to indicate stronger instability indices than ERA5. However, it is important to note that ERA5 data may not fully capture the environments favorable for isolated thunderstorms. The authors of [85] have shown that ERA5 tends to underestimate the upper tail of CAPE distributions, which are crucial for accurately representing such storm-prone environments. Similarly, ref. [82] also suggests that ERA5 tends to underestimate CAPE and other thermodynamic indices (TT and K) in convective environments, particularly in cases of shallow or slantwise convection. Hence, given the absence of upper-air observations for the region, ERA5 remains a valuable reference for comparison in this study. While all WRF simulations indicate favorable conditions for thunderstorms, it is unclear whether the model is overestimating instability or if ERA5 is underrepresenting the true atmospheric conditions.

In terms of vertical wind shear, it is weaker (<4 m s^{-1}) in the simulations compared to ERA5 (4–8 m s^{-1}). Despite the different configurations of the experiments, they exhibit a similar spatial pattern, with low values over the studied region (red box; Figure 10). On Table 4, among the simulations, the WDM6 microphysics scheme produced a shear value of 2.23 m s^{-1} for Itajubá, which was closest to the ERA5 reanalysis value of 4.82 m s^{-1}, whereas all other experiments yielded values below 2 m s^{-1}.

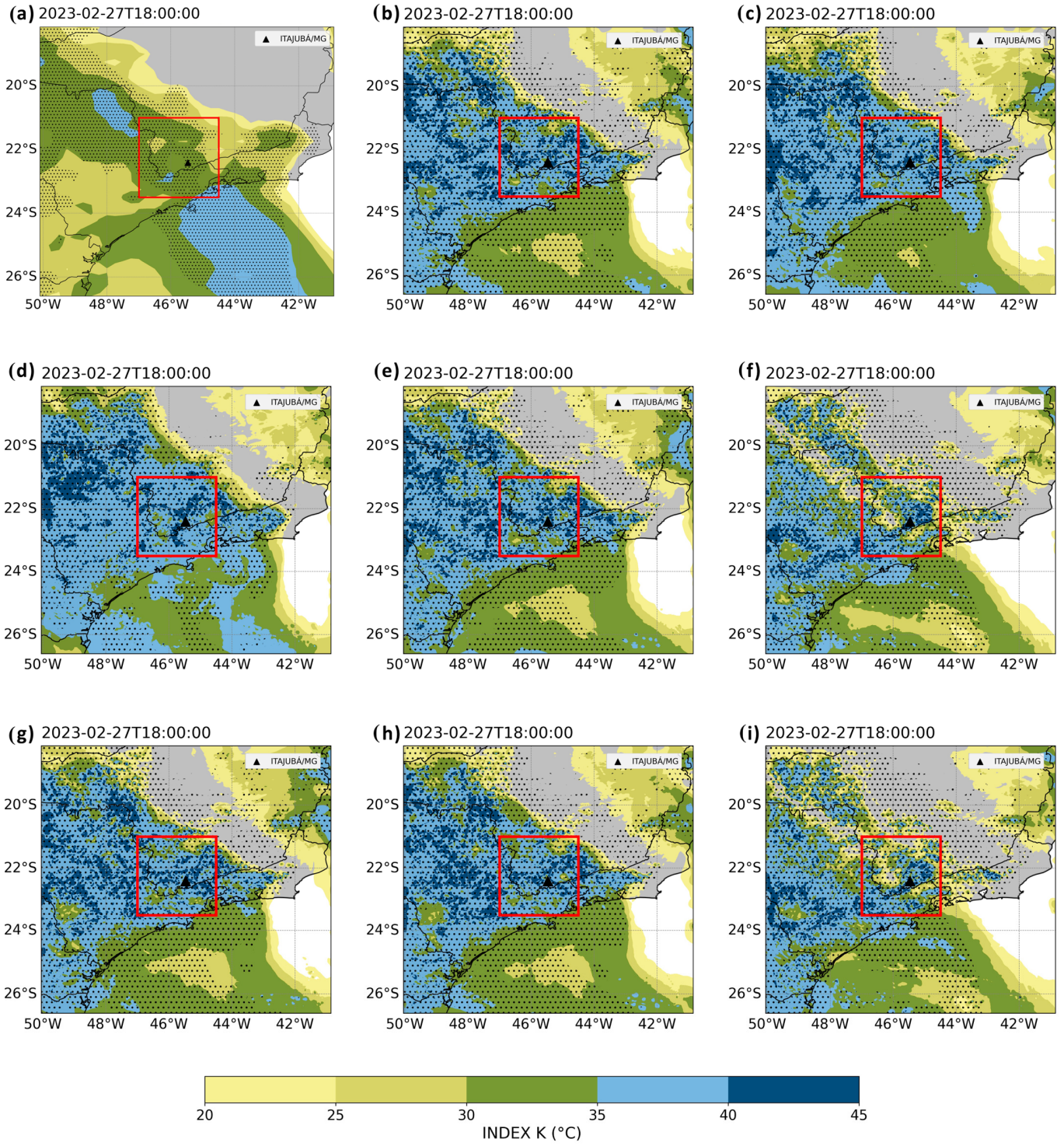


Figure 9. Total Totals Index (°C, dotted) higher than 44 °C and K Index (°C, shaded) on February 27 at 1800 UTC. Panels represent the following: (**a**) ERA5 reanalysis, (**b**) WSM3, (**c**) WSM6, (**d**) WDM6, (**e**) GDAS, (**f**) experiment using ERA5 data, (**g**) SST, (**h**) SOIL, and (**i**) ERA5_SST. The red box indicates the southern part of MG and northeast SP, and black triangle highlights the municipality of Itajubá.

While strong vertical wind shear is typically associated with organized and long-lived convective systems, thunderstorms can still develop in weak-shear environments, especially when a high CAPE is present [86–88], as is the case in this study. These storms are usually short-lived and less organized but can still produce severe weather phenomena. According to various studies [87,89], they typically last 45–60 min due to the weak vertical wind shear. In this situation, the precipitation core, filled with heavy hydrometeors, collapses

onto its updraft, and the updraft is undercut by cold outflow driven by the evaporation of precipitation, disrupting its source of potentially buoyant air.

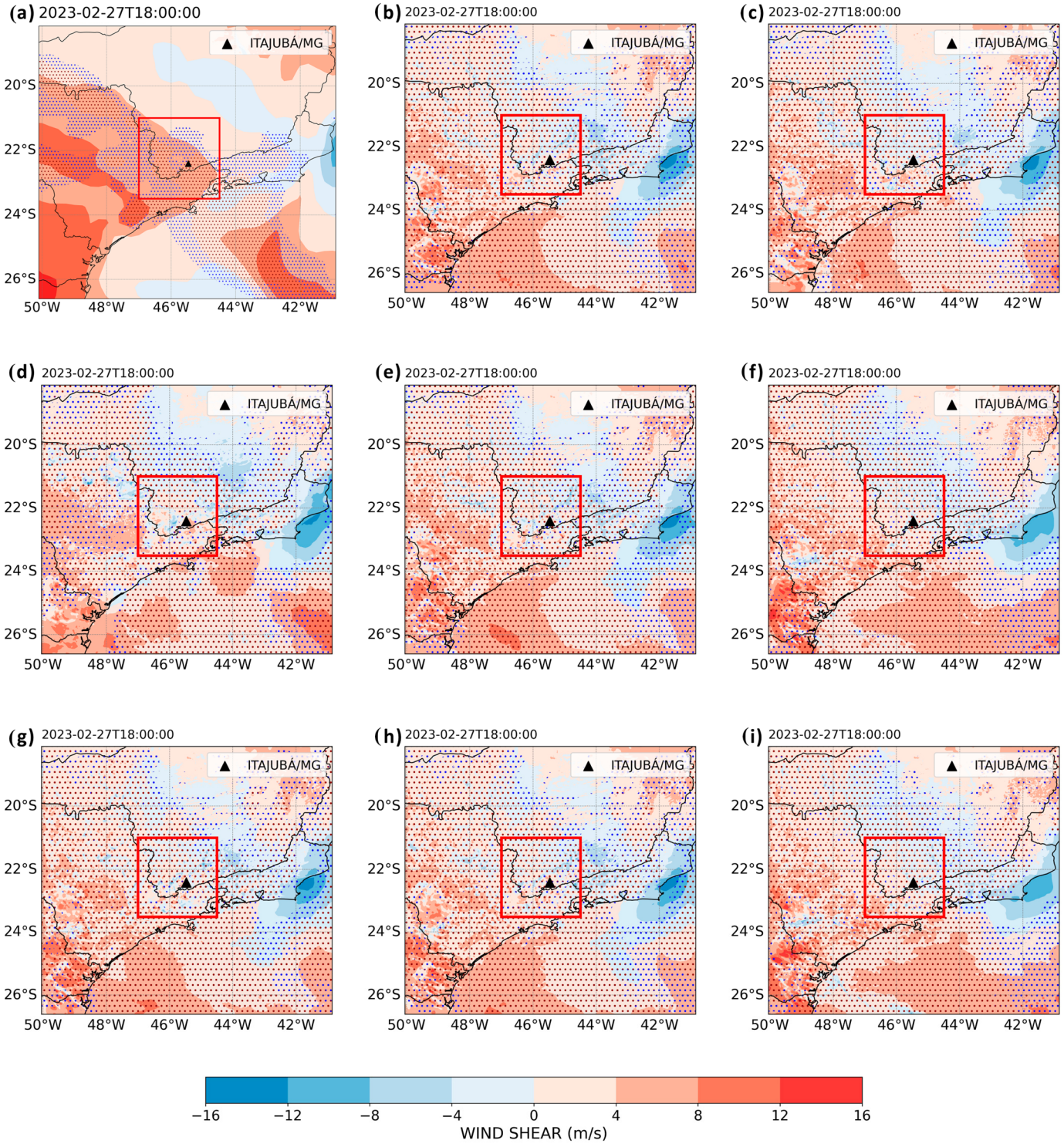


Figure 10. CAPE greater than 500 J kg^{-1} (dotted) and vertical wind shear between 500 and 1000 hPa (m s^{-1}, shaded) on February 27 at 1800 UTC. Panels represent the following: (**a**) ERA5 reanalysis data, (**b**) WSM3, (**c**) WSM6, (**d**) WDM6, (**e**) GDAS, (**f**) experiment with ERA5 data, (**g**) SST, (**h**) SOIL, and (**i**) ERA5_SST. The red box indicates the southern part of MG and northeast SP, and black triangle highlights the municipality of Itajubá.

The development of the studied storm over Itajubá despite weak vertical wind shear can be explained by the combination of other environmental factors, as shown in Section 3.1.

Over the region, the low-level atmospheric layer was wet: relative humidity at 850 hPa was higher than 80% and predominated the convergence of the vertically integrated moisture flux (Figure 6). The convergence associated with the convection due to the daytime warming (the air temperature reached high values in the afternoon, as observed by the meteorological station—31.4 °C) led to the atmospheric instability, as indicated by the various instability indices (Figures 9 and 10 and Table 4). The resulting thermodynamic conditions favored deep convection, leading to the formation and maintenance of the observed storm that was characterized by significant hydrometeor content. These findings reinforce the conclusion that the event under study is primarily influenced by thermodynamic rather than dynamic factors.

4. Conclusions

The main objective of this study was to evaluate the performance of the WRF model in simulating an extreme precipitation event that affected the Itajubá municipality in Minas Gerais (MG), southeastern Brazil, on 27 February 2023. To achieve this, eight numerical sensitivity experiments were conducted to test different physical configurations of the model, including cloud microphysics schemes, initial and boundary condition datasets, and surface parameters such as sea surface temperature (SST) and soil moisture. The main results are summarized below.

Key features of the storm: A rainband moving from northwest to southeast reached Itajubá, producing a high amount of precipitation (73 mm recorded at the UNIFEI station) within a short period (~40 min) in the afternoon of 27 February 2023. Due to these characteristics and indications of hail, the storm was classified as severe. Additionally, radar data (reflectivity above 30 dBZ) confirmed its convective nature and indicated a vertical extension of the storm of ~14 km.

Environmental Conditions Conducive to the Storm: The storm developed in a region with a lack of large-scale dynamic forcing for upward motion and weak vertical wind shear between 500 and 1000 hPa but under moist conditions, as indicated by relative humidity at 850 hPa exceeding 80% in southern MG and the convergence of the vertically integrated moisture flux (although not associated with a strong large-scale circulation pattern). These factors, combined with strong diurnal heating (maximum temperature reached 31.4 °C), created an unstable environment favorable for storm development. The instability was evidenced by thermodynamic indices, including TT (>44 °C), K (>30 °C), and CAPE (~1023 J kg^{-1}). Hence, the studied case exhibits a predominance of thermodynamic forcing.

Sensitivity Numerical Experiments: Although none of the simulations fully reproduced the observed spatial pattern of precipitation, likely due to the convective and local nature of the event combined with the complex topography of the region, some configurations yielded improved results. Among them, WSM3 showed slightly better agreement in representing the storm's thermodynamic environment, and the ERA5_SST experiment better matched the observed CAPE values. However, statistical performance remained weak overall. A central aspect of the analysis was the evaluation of atmospheric instability indices: TT, K index, and CAPE. The ERA5 reanalysis showed TT values above 45 °C, K around 33 °C, and CAPE exceeding 1000 J kg^{-1}. Those conditions indicate a moderately unstable atmosphere with a potential for convective development. The WRF simulations generally overestimated the instability, with some experiments showing CAPE values surpassing 1500 J kg^{-1} and K indices above 40 °C. Despite the high instability, vertical wind shear remained weak in all cases (<5 m s^{-1}), supporting the classification of the event as a short-lived and thermodynamically driven thunderstorm.

Model Configuration Considerations: Based on our results, we suggest that additional experiments tuning the microphysics scheme may help improve simulation results, partic-

ularly in cases where thermodynamic conditions play a more significant role than dynamic triggers. Our choice of WSM3, WSM6, and WDM6 was guided by operational constraints and previous experiments [33], which showed that WDM6 slightly outperformed other schemes in similar scenarios. However, we also recognize other advanced parameterization options and intend to explore them in future work.

Broader Implications: Although this study is limited to a single extreme event, the methodology adopted, including the sensitivity experiments with microphysics, boundary conditions, SST, and soil moisture, could be replicated for other extreme rainfall episodes in southeastern Brazil or in other places. Due to the region's complex terrain, future studies should explore how the WRF model performs under different weather conditions. However, this study reinforces that weak large-scale forcing does not preclude the existence of strong local orographic circulations, particularly in regions like the Mantiqueira Range. Previous work [59] has demonstrated that a 3 km WRF grid is capable of resolving thermally driven mountain–valley breezes in southeastern Brazil. Although we did not perform the dynamic diagnostics of slope circulations in the present study, the model resolution is consistent with literature that has successfully captured these fine-scale features using vertical cross-sections and time series.

Finally, the nesting configuration used (12 km → 3 km) reflects the current CEPreMG operational setup. However, we acknowledge the potential limitations of nesting, and we plan to conduct future experiments using single-domain, high-resolution simulations to assess the orographic and thermally driven processes. Should the results prove favorable, they will serve as a basis for improving the accuracy and robustness of CEPreMG's operational weather forecasting system. These sensitivity experiments can contribute to improving the model's configuration for better representation of extreme events, which can enhance early warning systems and provide critical information to local/regional governments and emergency management agencies, ultimately supporting more effective preparedness and response strategies to minimize the impacts on society.

Supplementary Materials: The following supporting information can be downloaded at https://www.mdpi.com/article/10.3390/atmos16050548/s1: Table S1 Instability indices used in the study. Table S2. Atmospheric situations associated with TT index. Adapted from [74]. Table S3. Atmospheric situations and occurrence probability associated with K index. Adapted from [72]. Table S4. Atmospheric situations associated with CAPE index. Adapted from [72]. Table S5. Thunderstorm type as a function of CAPE (J kg^{-1}) and vertical wind shear at 0–6 km (~1000 and 500 hPa) in m s^{-1}. Adapted from [88].

Author Contributions: Conceptualization, D.W.G. and M.S.R.; methodology, D.W.G., M.S.R. and V.S.B.C.; software, D.W.G.; formal analysis, D.W.G., M.S.R. and V.S.B.C.; writing—original draft preparation, D.W.G., M.S.R. and V.S.B.C.; writing—review and editing, D.W.G., M.S.R. and V.S.B.C. All authors have read and agreed to the published version of this manuscript.

Funding: This work was supported by the Brazilian agencies of Coordenação de Aperfeiçoamento de Pessoal de Nível Superior—Brasil (CAPES)—Financing Code 001, Conselho Nacional de Desenvolvimento Científico e Tecnológico (CNPq), and Fundação de Amparo à Pesquisa de Minas Gerais (FAPEMIG).

Institutional Review Board Statement: Not applicable.

Informed Consent Statement: Not applicable.

Data Availability Statement: All datasets used in this study are available on public online databases: CEMADEN: http://www2.cemaden.gov.br/mapainterativo/, ERA5: https://climate.copernicus.eu/climate-reanalysis, FCTH: https://www.saisp.br/estaticos/sitenovo/produtos.html, GDAS: https://www.ncei.noaa.gov/access/metadata/landing-page/bin/iso?id=gov.noaa.ncdc:C00379, GOES-16: https://noaa-goes16.s3.amazonaws.com/index.html, INMET: https://portal.inmet.gov.br/,

MERGE/CPTEC: http://ftp.cptec.inpe.br/modelos/tempo/MERGE/GPM, and CHIRPS: https://www.chc.ucsb.edu/data/chirps, all accessed on 28 April 2025.

Acknowledgments: The authors thank all meteorological centers that provided data for this study.

Conflicts of Interest: The authors declare no conflicts of interest.

References

1. IPCC. *Climate Change—Synthesis Report; Contribution of Working Groups I, II and III to the Fifth Assessment Report of the Intergovernmental Panel on Climate Change*; IPCC: Geneva, Switzerland, 2014.
2. Cassalho, F.; Beskow, S.; Vargas, M.M.; Moura, M.M.D.; Ávila, L.F.; Mello, C.R.D. Hydrological Regionalization of Maximum Stream Flows Using an Approach Based on L-Moments. *RBRH* **2017**, *22*, e27. [CrossRef]
3. Medeiros, R.M.D.; Sousa, E.P.D.; Gomes Filho, M.F. Ocorrência de Eventos Extremos de Precipitação em Campina Grande–Paraíba, Brasil. In Riscos Climáticos e Hidrológicos. 2014. Available online: https://www.riscos.pt/wp-content/uploads/2018/Outras_Pub/outros_livros/III_CIR/iii_cir_artigo074.pdf (accessed on 20 January 2024).
4. Bourdeau-Brien, M.; Kryzanowski, L. The Impact of Natural Disasters on the Stock Returns and Volatilities of Local Firms. *Q. Rev. Econ. Financ.* **2017**, *63*, 259–270. [CrossRef]
5. Reza, M. Urban Flood Modeling Using Hydrodynamic Models: A Case Study of Dhaka City. *J. Hydrol.* **2020**, *590*, 125448.
6. Freitas, C.M.; Silva, D.R.X.; Sena, A.R.M.; Silva, E.L.; Sales, L.B.F.; Carvalho, M.L.; Costa, A.M. Natural Disasters and Health: An Analysis of the Situation in Brazil. *Ciência Saúde Coletiva* **2014**, *19*, 3645. [CrossRef]
7. Hidalgo, J.; Baez, J. Impactos das Mudanças Climáticas nos Recursos Hídricos da América Latina. *Rev. Bras. de Climatol.* **2019**, *15*, 23–39.
8. Henneman, A.; Thornby, K.A.; Rosario, N.; Latif, J. Evaluation of Pharmacy Resident Perceived Impact of Natural Disaster on Stress During Pharmacy Residency Training. *Curr. Pharm. Teach. Learn.* **2020**, *12*, 147–155. [CrossRef]
9. Reichstein, M.; Bahn, M.; Ciais, P.; Frank, D.; Mahecha, M.D.; Seneviratne, S.I.; Wattenbach, M. Climate Extremes and the Carbon Cycle. *Nature* **2013**, *500*, 287–295. [CrossRef]
10. Zilli, M.T.; Carvalho, L.M.; Liebmann, B.; Silva Dias, M.A.F. A Comprehensive Analysis of Trends in Extreme Precipitation over Southeastern Coast of Brazil. *Int. J. Climatol.* **2017**, *37*, 2269–2279. [CrossRef]
11. Marrafon, V.H.; Reboita, M.S. Características da Precipitação na América do Sul Reveladas através de Índices Climáticos. *Rev. Bras. Climatologia* **2020**, *26*, 663. [CrossRef]
12. Lagos-Zúñiga, M.; Balmaceda-Huarte, R.; Regoto, P.; Torrez, L.; Olmo, M.; Lyra, A.; Pareja-Quispe, D.; Bettolli, M. Extreme indices of temperature and precipitation in South America: Trends and intercomparison of regional climate models. *Clim. Dyn.* **2024**, *62*, 4541–4562. [CrossRef]
13. Freitas, A.A.D.; Carvalho, V.S.B.; Reboita, M.S. Extreme Precipitation Events During the Wet Season of the South America Monsoon: A Historical Analysis over Three Major Brazilian Watersheds. *Climate* **2024**, *12*, 188. [CrossRef]
14. Gu, G.; Adler, R.F. Precipitation Intensity–Duration–Frequency Curves for the United States Based on the Global Precipitation Measurement (GPM) Mission. *J. Hydrometeorol.* **2022**, *23*, 789–805.
15. Bartolomei, F.R.; Ribeiro, J.G.M.; Reboita, M.S. Extreme Precipitation Events in Southeast Brazil: Summer 2021/2022. *Rev. Bras. Geogr. Física* **2023**, *16*, 2658–2676. [CrossRef]
16. Pinto, T.A.C.; Mattos, E.V.; Reboita, M.S.; de Souza, D.O.; Oda, P.S.S.; Martins, F.B.; Biscaro, T.S.; Ferreira, G.W.d.S. Synoptic and Mesoscale Atmospheric Patterns That Triggered the Natural Disasters in the Metropolitan Region of Belo Horizonte, Brazil, in January 2020. *Atmosphere* **2025**, *16*, 102. [CrossRef]
17. Alcântara, E.; Marengo, J.A.; Mantovani, J.; Londe, L.R.; San, R.L.Y.; Park, E.; Nobre, C. Deadly Disasters in Southeastern South America: Flash Floods and Landslides of February 2022 in Petrópolis, Rio de Janeiro. *Nat. Hazards Earth Syst. Sci.* **2023**, *23*, 1157–1175. [CrossRef]
18. Blaudt, L.M.; Alvarenga, T.W.; Garin, Y. Disaster Occurred in Petrópolis in the Summer of 2022: General Aspects and Civil Defense Data. *Geosciences* **2023**, *42*, 59–71. [CrossRef]
19. Oda, P.S.S.; Teixeira, D.L.S.; Pinto, T.A.C.; da Silva, F.P.; Riondet-Costa, D.R.T.; Mattos, E.V.; de Souza, D.O.; Bartolomei, F.; Reboita, M.; dos Santos, A.P.P. Disasters in Petrópolis, Brazil: Political, urban planning, and geometeorological factors that contributed to the event on February 15, 2022. *Urban Clim.* **2024**, *54*, 101849. [CrossRef]
20. Marengo, J.A.; Cunha, A.P.; Seluchi, M.E.; Camarinha, P.I.; Dolif, G.; Sperling, V.B.; Alcântara, E.H.; Ramos, A.M.; Andrade, M.M.; Stabile, R.A.; et al. Heavy Rains and Hydrogeological Disasters on February 18–19, 2023, in the City of São Sebastião, São Paulo, Brazil: From Meteorological Causes to Early Warnings. *Nat. Hazards* **2024**, *120*, 7997–8024. [CrossRef]
21. CEMADEN. Boletim de Impactos de Extremos de Origem Hidro-Geo-Climática. 2023. Available online: https://www.gov.br/cemaden/pt-br/assuntos/monitoramento/boletim-de-impactos (accessed on 29 June 2024).

22. da Rocha, R.P.; Reboita, M.S.; Crespo, N.M. Analysis of the Extreme Precipitation Event in Rio Grande do Sul between April and May 2024. *J. Health NPEPS* **2024**, *9*, 1–10. [CrossRef]
23. Reboita, M.S.; Mattos, E.V.; Capucin, B.C.; Souza, D.O.d.; Ferreira, G.W.d.S. A Multi-Scale Analysis of the Extreme Precipitation in Southern Brazil in April/May 2024. *Atmosphere* **2024**, *15*, 1123. [CrossRef]
24. Reboita, M.S.; Marietto, D.M.G.; Souza, A.B.; Barbosa, M. Caracterização atmosférica quando da ocorrência de eventos extremos de chuva na região sul de Minas Gerais. *Rev. Bras. Climatol.* **2017**, *21*, 1–17. [CrossRef]
25. Reboita, M.S.; Rodrigues, M.; Silva, L.F.; Alves, M.A. Aspectos climáticos do estado de Minas Gerais. *Rev. Bras. Climatol.* **2015**, *17*, 206–226. [CrossRef]
26. Teodoro, T.A.; Reboita, M.S.; Llopart, M.; da Rocha, R.P.; Ashfaq, M. Climate change impacts on the South American monsoon system and its surface–atmosphere processes through RegCM4 CORDEX-CORE projections. *Earth Syst. Environ.* **2021**, *5*, 825–847. [CrossRef]
27. Ferreira, G.W.S.; Reboita, M.S. A new look into the South America precipitation regimes: Observation and forecast. *Atmosphere* **2022**, *13*, 873. [CrossRef]
28. Campos, B.; Carvalho, V.S.B.; Calheiros, A.J.P. Análise da ocorrência de eventos extremos de precipitação registrados no município de Itajubá, MG. In *Anais do XIX Congresso Brasileiro de Meteorologia*; Sociedade Brasileira de Meteorologia: João Pessoa, Brasil, 2011.
29. Pinheiro, M.V. Avaliação técnica e histórica das enchentes em Itajubá–MG. Master's Thesis, Universidade Federal de Itajubá, Itajubá, Brazil, 2005.
30. G1. Universidade Federal de Itajubá Estima Prejuízo de R$ 3 Milhões com Chuva que Invadiu 70% do Campus. Available online: https://g1.globo.com/mg/sul-de-minas/noticia/2023/02/28/universidade-federal-de-itajuba-estima-prejuizo-de-r-3-milhoes-com-chuva-que-invadiu-70percent-do-campus.ghtml (accessed on 20 June 2023).
31. Mohan, P.R.; Srinivas, C.V.; Yesubabu, V.; Baskaran, R.; Venkatraman, B. Simulation of a heavy rainfall event over Chennai in Southeast India using WRF: Sensitivity to microphysics parameterization. *Atmos. Res.* **2018**, *210*, 83–99. [CrossRef]
32. Liu, D.; Yang, B.; Zhang, Y.; Qian, Y.; Huang, A.; Zhou, Y.; Zhang, L. Combined impacts of convection and microphysics parameterizations on the simulations of precipitation and cloud properties over Asia. *Atmos. Res.* **2018**, *212*, 172–185. [CrossRef]
33. Campos, B.; Carvalho, V.S.B.; Mattos, E.V. Assessment of cloud microphysics and cumulus convection schemes to model extreme rainfall events over the Paraíba do Sul River Basin. *Urban Clim.* **2023**, *51*, 101618. [CrossRef]
34. Solano-Farias, J.; Ojeda, M.G.-V.; Donaire-Montaño, D.; Rosa-Cánovas, J.J.; Castro-Díez, Y.; Esteban-Parra, M.J.; Gámiz-Fortis, S.R. Assessment of physical schemes for WRF model in convection-permitting mode over southern Iberian Peninsula. *Atmos. Res.* **2024**, *299*, 107175. [CrossRef]
35. Souza, L.S.; da Silva, M.S.; de Almeida, V.A.; Moraes, N.O.; de Souza, E.P.; Senna, M.C.A.; Viana, L.Q. Evaluation of cumulus and microphysical parameterization schemes of the WRF model for precipitation prediction in the Paraíba do Sul River Basin, southeastern Brazil. *Pure Appl. Geophys.* **2024**, *181*, 679–700. [CrossRef]
36. Faria, L.F.; Reboita, M.S.; Mattos, E.V.; Carvalho, V.S.B.; Ribeiro, J.G.M.; Capucin, B.C.; Drummond, A.; Santos, A.P.P. Synoptic and mesoscale analysis of a severe weather event in southern Brazil at the end of June 2020. *Atmosphere* **2023**, *14*, 486. [CrossRef]
37. Gunwani, P.; Govardhan, G.; Jena, C.; Yadav, P.; Kulkarni, S.; Debnath, S.; Ghude, S.D. Sensitivity of WRF/Chem simulated PM2.5 to initial/boundary conditions and planetary boundary layer parameterization schemes over the Indo-Gangetic Plain. *Environ. Monit. Assess.* **2023**, *195*, 560. [CrossRef]
38. Duzenli, E.; Yucel, I.; Yilmaz, M.T. Evaluation of the fully coupled WRF and WRF-Hydro modelling system initiated with satellite-based soil moisture data. *Hydrol. Sci. J.* **2024**, *69*, 691–708. [CrossRef]
39. Prefeitura Municipal de Itajubá. Aspectos Físicos e Geográficos. Available online: https://itajuba.mg.gov.br/cidade/aspectos-fisicos-e-geograficos/ (accessed on 20 June 2023).
40. Minuzzi, R.B.; Sediyama, G.C.; Barbosa, E.D.M.; Melo Júnior, J.C.F. Climatologia do comportamento do período chuvoso da região sudeste do Brasil. *Rev. Bras. de Meteorol.* **2007**, *22*, 338–344. [CrossRef]
41. Siqueira, H.R.; Alves, G.D.F.; Guimarães, E.C. Comportamento da precipitação pluviométrica mensal do Estado de Minas Gerais: Análise espacial e temporal. *Horiz. Científico* **2007**, *1*, 1–15.
42. Viola, M.R.; Mello, C.R.; Pinto, D.B.; Mello, J.M.; Ávila, L.F. Métodos de interpolação espacial para o mapeamento da precipitação pluvial. *Rev. Bras. Eng. Agrícola E Ambient.* **2010**, *14*, 970–978. [CrossRef]
43. Souza, L.R.; Amanajás, J.C.; Silva, A.P.N.; Braga, C.C.; Correia, M.F. Determinação de padrões espaço-temporal e regiões homogêneas de precipitação pluvial no estado de Minas Gerais. *Eng. Ambient. Pesqui. Tecnol.* **2011**, *8*, 265–280.
44. Mello, L.G.N.; Viola, M.R. Modelagem hidrológica aplicada à previsão de cheias em bacias urbanas. *Rev. Bras. Recur. Hídricos* **2013**, *18*, 215–226.
45. Silva, L.J.; Reboita, M.S.; da Rocha, R.P. Relação da passagem de frentes frias na região sul de Minas Gerais com a precipitação e eventos de geada. *Rev. Bras. Climatol.* **2014**, *14*, 100–115. [CrossRef]
46. Hersbach, H.; Bell, B.; Berrisford, P.; Hirahara, S.; Horányi, A.; Muñoz-Sabater, J.; Nicolas, J.; Peubey, C.; Radu, R.; Schepers, D.; et al. The ERA5 Global Reanalysis. *Q. J. R. Meteorol. Soc.* **2020**, *146*, 1999–2049. [CrossRef]

47. NOAA. Global Data Assimilation System (GDAS) and Global Forecast System (GFS). 2025. Available online: https://www.ncei.noaa.gov/products/weather-climate-models/global-forecast (accessed on 10 January 2025).
48. Rodriguez, C.A.M. *Estratégias de Varredura para o Radar Meteorológico do CLA*; Instituto de Aeronáutica e Espaço: São José dos Campos, Brazil, 2020.
49. Houze, R.A. *Cloud Dynamics*; Academic Press: San Diego, CA, USA, 1993.
50. Bringi, V.N.; Chandrasekar, V. *Polarimetric Doppler Weather Radar: Principles and Applications*; Cambridge University Press: Cambridge, UK, 2001.
51. Steiner, M.; Houze, R.A.; Yuter, S.E. Climatological characterization of three-dimensional storm structure from operational radar and rain gauge data. *J. Appl. Meteorol.* **1995**, *34*, 1978–2007. [CrossRef]
52. Rozante, J.R.; Moreira, D.S.; Gonçalves, L.G.G.; Carvalho, L.M.V. A technique for merging satellite and conventional rainfall observations: Application over South America. *J. Hydrometeorol.* **2010**, *11*, 1140–1153. [CrossRef]
53. Huffman, G.J.; Bolvin, D.T.; Joyce, R.; Kelley, O.A.; Nelkin, E.J.; Tan, J.; Watters, D.C.; West, B. *Integrated Multi-satellite Retrievals for GPM (IMERG) Technical Documentation*; NASA Goddard Space Flight Center: Greenbelt, MD, USA, 2023. Available online: https://gpm.nasa.gov/sites/default/files/2023-07/IMERG_TechnicalDocumentation_final_230713.pdf (accessed on 29 January 2024).
54. Funk, C.; Peterson, P.; Landsfeld, M.; Pedreros, D.; Verdin, J.; Shukla, S.; Husak, G.; Rowland, J.; Harrison, L.; Hoell, A.; et al. The climate hazards infrared precipitation with stations—A new environmental record for monitoring extremes. *Sci. Data* **2015**, *2*, 150066. [CrossRef] [PubMed]
55. Skamarock, W.C. *A Description of the Advanced Research WRF Version 4*; NCAR Technical Note NCAR/TN-556+STR; National Center for Atmospheric Research: Boulder, CO, USA, 2019.
56. Skamarock, W.C.; Klemp, J.B. A Time-Split Nonhydrostatic Atmospheric Model for Weather Research and Forecasting Applications. *J. Comput. Phys.* **2008**, *227*, 3465–3485. [CrossRef]
57. Araújo, A.A.; Garcia, D.W.; Monteiro, J.R.; Miguel, T.V.; Campos, B.; Carvalho, V.S.B.; Reboita, M.S. Avaliação do modelo WRF na simulação operacional de um evento de frente fria no sudeste do Brasil. *Rev. Bras. Geogr. Física* **2023**, *16*, 805–817. [CrossRef]
58. Garcia, D.W.; Reboita, M.S.; Carvalho, V.S.B. Evaluation of WRF Performance in Simulating an Extreme Precipitation Event Over the South of Minas Gerais, Brazil. *Atmosphere* **2023**, *14*, 1276. [CrossRef]
59. Campos, B.; Reboita, M.S.; Carvalho, V.S.B.; Dias, C.G. Circulações Locais Induzidas pela Topografia no Vale do Paraíba e na Serra da Mantiqueira: Um estudo de caso para o período entre os dias 16 e 22 de agosto de 2010. *Rev. Bras. Geogr. Física* **2016**, *9*, 753–765. [CrossRef]
60. Freitas, E.D.; Rozoff, C.M.; Cotton, W.R.; Dias, P.L.S. Interactions of an urban heat island and sea-breeze circulations during winter over the metropolitan area of São Paulo, Brazil. *Bound.-Layer Meteorol.* **2007**, *122*, 43–65. [CrossRef]
61. Grell, G.A.; Freitas, S.R.; Stuefer, M.; Fast, J.D. Inclusion of Biomass Burning in WRF-Chem: Impact of Wildfires on Weather Forecasts. *Atmos. Chem. Phys.* **2014**, *14*, 527–552. [CrossRef]
62. Hong, S.Y.; Dudhia, J.; Chen, S.H. A Revised Approach to Ice Microphysical Processes for the Bulk Parameterization of Cloud and Precipitation. *Mon. Weather Rev.* **2004**, *132*, 103–120. [CrossRef]
63. Hong, S.-Y.; Lim, J.-O.J. The WRF Single-Moment 6-Class Microphysics Scheme (WSM6). *J. Korean Meteorol. Soc.* **2006**, *42*, 129–151.
64. Jiménez, P.A.; Dudhia, J.; González-Rouco, J.F.; Navarro, J.; Montávez, J.P.; García-Bustamante, E. A Revised Scheme for the WRF Surface Layer Formulation. *Mon. Weather Rev.* **2012**, *140*, 898–918. [CrossRef]
65. Tewari, M.; Chen, F.; Wang, W.; Dudhia, J.; LeMone, M.A.; Mitchell, K.; Ek, M.; Gayno, G.; Wegiel, J.; Cuenca, R.H. Implementation and Verification of the Unified Noah Land Surface Model in the WRF Model. In Proceedings of the 20th Conference on Weather Analysis and Forecasting/16th Conference on Numerical Weather Prediction, Seattle, WA, USA, 12–16 January 2004; American Meteorological Society: Boston, MA, USA, 2004.
66. Dudhia, J. Numerical Study of Convection Observed During the Winter Monsoon Experiment Using a Mesoscale Two-Dimensional Model. *J. Atmos. Sci.* **1989**, *46*, 3077–3107. [CrossRef]
67. Mlawer, E.J.; Taubman, S.J.; Brown, P.D.; Iacono, M.J.; Clough, S.A. Radiative Transfer for Inhomogeneous Atmospheres: RRTM, a Validated Correlated-k Model for the Longwave. *J. Geophys. Res. Atmos.* **1997**, *102*, 16663–16682. [CrossRef]
68. Lim, J.O.J.; Hong, S.Y. Development of an Effective Double-Moment Cloud Microphysics Scheme with Prognostic Cloud Condensation Nuclei (CCN). *J. Atmos. Sci.* **2010**, *67*, 1308–1315. [CrossRef]
69. Lin, Y.L.; Farley, R.D.; Orville, H.D. Bulk Parameterization of the Snow Field in a Cloud Model. *J. Clim. Appl. Meteorol.* **1983**, *22*, 1065–1092. [CrossRef]
70. Dudhia, J.; Gill, D.; Manning, K.W.; Wang, W.; Bruyere, C.L. *PSU/NCAR Mesoscale Modeling System Tutorial Class Notes and User's Guide*; National Center for Atmospheric Research: Boulder, CO, USA, 2008.
71. Jackson, B.M.; Kavetski, D.; Franks, S.W. Bayesian Estimation of Hydrological Model Parameters and Uncertainty. *Water Resour. Res.* **2019**, *55*, 10866–10881. [CrossRef]
72. Vasquez, M.C. *Severe Storm Forecasting*; National Weather Service: Silver Spring, MD, USA, 2017.

73. George, J.J. *Weather Forecasting for Aeronautics*; Academic Press: New York, NY, USA, 1960.
74. Miller, R.C. *Notes on Analysis and Severe-Storm Forecasting Procedures of the Air Force Global Weather Central*; AWS Tech. Rep. 200; Air Weather Service (MAC), USAF: Scott AFB, IL, USA, 1972.
75. Delgado, R.C.; Santos, E.O. Precipitation. In *Basic Meteorology Handbook—IF 111—2013—DCA/IF/UFRRJ*; 2013; p. 245. Available online: https://doceru.com/doc/n5c1n85 (accessed on 26 June 2024).
76. Doswell, C.A., III. The distinction between large-scale and mesoscale contribution to severe convection: A case study example. *Weather. Forecast.* **1987**, *2*, 3–16. [CrossRef]
77. Wallace, J.M.; Hobbs, P.V. *Atmospheric Science: An Introductory Survey*; Academic Press: San Diego, CA, USA, 2006.
78. Ahrens, C.D.; Henson, R. *Meteorology Today: An Introduction to Weather, Climate, and the Environment*; Cengage Learning: Boston, MA, USA, 2015.
79. Weisman, M.L.; Klemp, J.B. The Dependence of Numerically Simulated Convective Storms on Vertical Wind Shear and Buoyancy. *Mon. Weather Rev.* **1982**, *110*, 504–520. [CrossRef]
80. Campos, B. Sensibilidade de Parametrizações de Convecção Cumulus e Microfísica de Nuvens em Eventos Extremos de Precipitação na Bacia do Rio Paraíba do Sul. Master's Thesis, Programa de Pós-Graduação em Meio Ambiente e Recursos Hídricos, Universidade Federal de Itajubá (UNIFEI), Itajubá, Brazil, 2022.
81. Jeworrek, J.; Barthlott, C.; Hoose, C. The Influence of Orography on Precipitation Patterns: Idealized Simulations and Observations. *Atmos. Res.* **2021**, *256*, 105561. [CrossRef]
82. Yavuz, V. Variations in Air Pollutant Concentrations on Dry and Wet Days with Varying Precipitation Intensity. *Atmosphere* **2024**, *15*, 896. [CrossRef]
83. NOAA. Severe Weather Event Guide. National Oceanic and Atmospheric Administration. 2025. Available online: https://www.noaa.gov/severe-weather-guide (accessed on 20 April 2025).
84. Henry, R. Thunderstorm Forecasting Using Stability Indices. *Weatherwise* **1987**, *40*, 94–100.
85. Wu, J.; Guo, J.; Yun, Y.; Yang, R.; Guo, X.; Meng, D.; Chen, T. Can ERA5 reanalysis data characterize the pre-storm environment? *Atmos. Res.* **2024**, *297*, 107108. [CrossRef]
86. Weisman, M.L.; Klemp, J.B. The structure and classification of numerically simulated convective stormsin directionally varying wind shears. *Mon. Weather Rev.* **1984**, *112*, 2479–2498. [CrossRef]
87. Markowski, P.; Richardson, Y. *Mesoscale Meteorology in Midlatitudes*; Wiley-Blackwell: Chichester, UK, 2010.
88. Joe, P.; Dance, S.; Lakshmanan, V.; Heizenreder, D.; James, P.; Lang, P.; Hengstebeck, T.; Feng, Y.; Li, P.W.; Yeung, H.-Y.; et al. Automated processing of doppler radar data for severe weather warnings. In *Doppler Radar Observations: Weather Radar, Wind Profiler, Ionospheric Radar, and Other Advanced Applications*; InTech: Houston, TX, USA, 2012; pp. 33–74.
89. Pucik, T.; Groenemeijer, P.; Tijssen, L.; Holzer, A.M. The Environments of Severe Thunderstorms over Europe. *Mon. Weather Rev.* **2021**, *149*, 1793–1811.

Disclaimer/Publisher's Note: The statements, opinions and data contained in all publications are solely those of the individual author(s) and contributor(s) and not of MDPI and/or the editor(s). MDPI and/or the editor(s) disclaim responsibility for any injury to people or property resulting from any ideas, methods, instructions or products referred to in the content.